Process Biochemistry 119 (2022) 106–118

Contents lists available at ScienceDirect

Process Biochemistry

journal homepage: www.elsevier.com/locate/procbio

Apoptotic, antioxidant and cytotoxic properties of synthesized AgNPs using green tea against human testicular embryonic cancer stem cells

Fahimeh Mobaraki [a], Mohsen Momeni [b], Maliheh Jahromi [c], Farshad Moharrami Kasmaie [d], Maryam Barghbani [e], Mohammad Ehsan Taghavizadeh Yazdi [f], Zahra Meshkat [g], Fatemeh Homaee Shandiz [h], Seyed Mousalreza Hosseini [i,j,*]

[a] Department of Anatomy and Cell Biology, School of Medicine, Mashhad University of Medical Sciences, Mashhad, Iran
[b] Immuno-Biochemistry lab, Immunology Research Center, Mashhad University of Medical Sciences, Mashhad, Iran
[c] Department of Medicine, Najafabad Branch, Islamic Azad University, Najafabad, Iran
[d] Department of Biology and Anatomical Sciences, School of Medicine, Shahid Beheshti University of Medical Sciences, Tehran, Iran
[e] Department of Medical Biotechnology, School of Allied Medicine, Qazvin University of Medical Sciences, Qazvin, Iran
[f] Applied Biomedical Research Center, School of Medicine, Mashhad University of Medical Sciences, Mashhad, Iran
[g] Department of Microbiology and Virology, School of Medicine, Mashhad University of Medical Sciences, Mashhad, Iran
[h] Cancer Research Center, Mashhad University of Medical Sciences, Mashhad, Iran
[i] Department of Gastroenterology, School of Medicine, Mashhad University of Medical Sciences, Mashhad, Iran
[j] Surgical Oncology Research Center, Mashhad University of Medical Sciences, Mashhad, Iran

ARTICLE INFO

Keywords:
Biosynthesis
Camellia sinensis
Apoptosis
NTERA-2
Cancer therapy

ABSTRACT

Silver nanoparticles (AgNPs) are known as carriers of anticancer activities for effectual target treatment of cancer cells. Plant-mediated synthesis for AgNPs synthesis is valuable for biomedical applications due to their more safety and cost-effectiveness. In this work, AgNPs were synthesized successfully using green tea (*Camellia sinensis)* extract (CSE-AgNPs). The physicochemical properties of CSE-AgNPs were identified by UV–visible spectrophotometry, FT-IR, PXRD, DLS and TEM. The results indicated the successful synthesis of well-dispersed CSE-AgNPs with spherical shape and size (8–68 nm). The cytotoxic effects of CSE-AgNPs on hominid testicular embryonic cancer stem cells (NTERA-2) and normal cells (ACTH2 cell line) were done by the MTT assay and acridine orange/propidium iodide staining. CSE-AgNPs exhibited toxic effects in a dose-dependent manner as their half inhibitory concentrations (IC50) were 6 μg/mL and 28 μg/mL against the cancerous and normal cells after 24 h, respectively. The investigation of Bcl2, Bax, caspase 3 and 9, p53 and HSPA2 genes' expression indicated CSE-AgNPs as an apoptosis-inducing complex. The findings document the usability of the bio-synthesized CSE-AgNPs for triggering cell death in cancerous cells in vitro and provide a strong rationale for conducting in vivo studies.

1. Introduction

Cancer is a generic term denoting a large group of diseases, in which the organization's cells begin to propagate and reproduce uncontrollably [1–6]. The rapid growth of cancerous cells leads to the formation of abnormal tissues identified as malignant tumors [7–12] which can attack healthy organs and tissues [13–18]. The development of civilization and commercial expansion causes an alteration in dietary forms and, in the meantime, plants and biomaterials derived from the plant can help improve health [19–24]. Testicular cancer is a common form of cancer among men aged 15–34 years old, accounting for about 8850 new cases and 410 deaths in 2017 in the USA [25]. Medical treatment of testicular cancer generally includes orchiectomy, radiation therapy and chemotherapy. These approaches, alone or together, have proved effective to some extent. Still, there are critical limitations to the mentioned therapies, including their serious side effects for healthy tissues or organs, hypogonadism and metabolic syndrome [26]. Therefore, developing novel therapies with the lowest side effects is of utmost clinical importance [27,28]. Nanotechnology holds promises for cancer theranostics by enabling the synthesis of materials and devices with higher efficacy and lower adverse effects on normal cells and tissues [29–31]. Nanoparticle-targeted therapy is a helpful technique for cancer

* Corresponding author at: Department of Gastroenterology, School of Medicine, Mashhad University of Medical Sciences, Mashhad, Iran.
E-mail address: Hoseinimr@mums.ac.ir (S.M. Hosseini).

https://doi.org/10.1016/j.procbio.2022.05.021
Received 30 December 2021; Received in revised form 22 May 2022; Accepted 24 May 2022
Available online 26 May 2022

therapy since the particles can effectively penetrate the tumor tissue, leading to the accumulation of therapeutic agents at the tumor site [32–34]. Among metallic nanoparticles, silver nanoparticles (AgNPs) are important and attractive nano-sized materials in biology and medicine [35,36]. AgNPs are commonly identified as potential anticancer substances due to their inherent capacity in the inhibition of tumor cell propagation, migration and angiogenesis [37,38]. AgNPs can also cross the blood-testis and blood-brain barriers to reach tumor regions [39]. However, the conventional approaches adopted for the fabrication of nanoparticles (NPs) suffers from the existence of some toxic chemicals adsorbed on the particles' surface, seriously hindering their medical applications [40]. Therefore, the biosynthesis of nanoparticles, known as green chemistry synthesis, has been proposed to produce nano-sized particles in a simple, rapid, dependable and non-toxic manner [41].

Chemical and physical methods are time-consuming and not eco-friendly [42,43]; an environmentally safe approach to the synthesis of NPs is the biological method [44,45]. Different biological systems, including bacteria, fungi and herbal extracts, have been successfully employed for the biosynthesis of metallic NPs [46]. Studies have reported the role of metabolites such as terpenoids, flavonoids, carbohydrates, proteins and phenolic compounds in the synthesis of NPs [34]. These agents are responsible for the formation of nanoparticles by reducing properties, thereby promoting their stabilizing characteristics and biocompatibility [47–49]. Researchers have identified plants that have a high potential for synthesizing silver nanoparticles, e.g., turmeric, *Nigella sativa* [47], *Zingiber officinale* [50] and black tea [51]. In this regard, green tea (*Camellia sinensis*) leaf, as a strong antioxidant and chemopreventive agent, has been proved as an affordable choice for the green chemistry synthesis of nanoparticles [52].

In the current research, for the first time, we demonstrate the enhanced anticancer activity of AgNPs biosynthesized by *C. sinensis* (CSE-AgNPs) against human testicular carcinoma cells (NTERA-2). For this purpose, *C. sinensis* was first extracted from a leaf of wild-growing green tea. Then, the extract was utilized for the biofabrication of AgNPs using a biochemical procedure. The fully characterized samples were evaluated biologically to determine their exact anticancer efficacy both at the cellular and molecular levels.

2. Experimental procedure

2.1. Materials

Silver nitrate ($AgNO_3$), sodium hydroxide (NaOH) and hydrochloric acid (HCl) were obtained from Merck KGaA (Germany). The cell culture medium (DMEM/F12), FBS, PBS, penicillin and streptomycin were procured from Invitrogen (USA). Trypsin, ethylene diamine tetraacetic acid (EDTA), DAPI and MTT were obtained from Sigma-Aldrich (United States).

2.2. Plant extract preparation and biosynthesis of AgNPs

The leaves of wild-growing *C. sinensis* were collected from villages of Rudsar, north of Iran. The samples were then washed twice with deionized water. Freshly dried leaves were ground into fine powder under a sterile position. To prepare the *C. sinensis* extract, 1 g of the powder was solved in deionized water (100 mL) and, then, stirred for 30 min. The solution was filtered (Whatman no. 42 paper) and stored at 4 °C [53]. This extract was considered as a concentration of 100% and other concentrations were made from this base extract solution.

For the biosynthesis of AgNPs, 3 mL of the prepared extract was dropped into 7 mL of the $AgNO_3$ solution (1 mM). The UV absorption spectra of the solution were determined between 300 and 900 nm using UV–Vis spectroscopy (Japan's Shimadzu UV-2500 model). Different factors were assessed to achieve nanoparticles with suitable size and stability [54].

2.3. Optimizing effective parameters in the biosynthesis of AgNPs

To optimize the pH of CSE-AgNPs, 3 mL of the extract and 7 mL of $AgNO_3$ solution were mixed in six tubes. Then, pH was set to 4, 5, 6, 7, 8 and 9 using HCl (0.1 M) and NaOH (0.1 M). The absorption spectra of all the colloidal solutions were assessed by a spectrophotometer (Shimadzu UV-2500) in the series of 300–900 nm and the optimal pH was selected. The $AgNO_3$ solution and plant extract were used at various ratios of 1:9 (1 mL $AgNO_3$ /9 mL extract), 2:8 (2 mL $AgNO_3$ /8 mL extract), 3:7 (3 mL $AgNO_3$ /7 mL extract), 4:6 (4 mL $AgNO_3$ /6 mL extract), 1:9 (1 mL extract /9 mL $AgNO_3$), 2:8 (2 mL extract /8 mL $AgNO_3$), 3:7 (3 mL extract /7 mL $AgNO_3$) and 6:4 (6 mL extract/4 mL $AgNO_3$) to optimize nanoparticle preparation. The absorption spectra of CSE-AgNPs at all ratios were evaluated by UV–Vis spectroscopy. Then, the optimum ratio of the plant extract to the $AgNO_3$ solution was applied to produce CSE-AgNPs. To optimize the reaction time, the absorption spectra of CSE-AgNPs were determined at different times (30, 60, 120, 180 and 240 min) and the optimal time was specified.

2.4. Physicochemical characterizations

For physicochemical characterization, the CSE-AgNPs solution was first centrifuged three times at 12,000 rpm for 15 min and, then, freeze-dried. To determine crystalline phases, the obtained powder was introduced into an X-ray diffractometer (Philips X′pert Pro, the Netherlands) with Cukα radiation ($\lambda = 1.5406$ Å) in the series of 10–80° with 2°/min scanning degree. FTIR examination was performed to detect the surface functional groups as well as the stretching and bending vibrations in the green tea extract powder and AgNPs. The FT-IR spectra of the examples were documented in the wavenumber range of 500–4000 cm^{-1} using a smart diffuse reflectance FT-IR (NICOLET IR 100 model). The particle size distribution profile of the CSE-AgNPs was investigated using a DLS (Photal, Otsuka Electronics Co.). The structural investigation of the CSE-AgNPs was performed by a transmission electron microscope (TEM) (LEO - 912AB - 120 KV model, Carl Zeiss, Germany). Image J software was employed to analyze the micrographs and the particle size distribution.

2.5. Biological evaluations

2.5.1. Antioxidant property

The antioxidant activity of the CSE-AgNPs was identified using the ABTS-radical scavenging and DPPH free radical scavenging assays. Briefly, 54.8 mg of ABTS (2 mM) was dissolved in 50 mL of distilled water, added along with 0.3 mL of potassium persulphate (17 mM) and kept at 37 °C for 24 h. Then, 1 mL of DMSO and 0.16 mL of ABTS solution were added to 0.2 mL of different concentrations of the samples to create the final solution. After 20 min, absorbance was calculated by using an ultraviolet–spectrophotometer at 734 nm [55].

In the DPPH assay, each sample was diluted in water in 96-well microtitre plates separately and the final concentrations of the plant extract, AgNPs and standard solution were attained (1.56, 3.12, 6.25, 12.5, 25, 50 and 100 μg/mL). Afterwards, 200 μl of the DPPH solution was added to 2.5 mL of the example solution. The plates were incubated at 37 °C for 30 min and the absorbance was measured at 490 nm. Ascorbic acid (routine) was applied as the control (+) and the extract was employed as the blank.

The percentage of inhibition was designed as stated by the subsequent equation [14]:

$$\text{Percentage of inhibition} = \frac{\text{Absorption control} - \text{Absorption test}}{\text{Absorption control}} \times 100$$

2.5.2. Cell culture

Pluripotent humanoid testicular embryonic cancer stem cells (NTERA-2 Cell No: IBRC C10509) and normal human testis (ACTH2 Cell

No: IBRC C11135) cell lines were purchased from Iran Biological Resource Center (Iran). The NTERA-2 and ACTH2 cell lines were cultured in the DMEM medium modified with L-Glutamine, 15% FBS, 1% P/S at 37 °C in humid air with 5% CO_2. Once reaching at least 70% confluency, the cells were separated from the cell culture flasks by 5% trypsin–EDTA solution and utilized for the cytocompatibility assay.

2.5.3. In vitro cyto-compatibility of CSE-AgNPs

The effect of CSE-AgNPs on the growth and proliferation of NTERA-2 and ACTH2 cell lines was done by the MTT assay which is a colorimetric method. This method is established on the disintegration of tetrazolium salt in viable cells. The NTERA-2 and ACTH2 cells were plated into 96-well culture plates containing 100 µl of the culture medium separately. Then, CSE-AgNPs were added to each well with different treatments (0, 0.78, 1.56, 3.12, 6.25, 12.5, 25, 50 and 100 µg/mL). After 24 h, 100 µl of the MTT solution (0/5 µg/mL) was added to each well and incubated for 4 h at 37 °C. Afterwards, the medium containing MTT was discarded and DMSO was added to each well for 30 min. The light absorption of each well was read by an ELISA reader at 570 nm. The results were defined as an IC50% (50% maximal inhibitory concentration). To achieve better results, the assessments were repeated three times and the ratio of viable cells was calculated by the following procedure [56,57]:

$$\text{Percentage of cell vitality}(\%) = \frac{\text{Mean absorbance of the treated sample}}{\text{Mean absorbance of the control sample}} \times 100$$

2.5.4. AO/PI staining assay

NTERA-2 and ACTH2 cell lines were seeded in 6–well cell culture microplates (SPL Lifescience). The NTERA-2 cells (1×10^6 cells/mL) were treated with 6 and 12.5 µg/mL of the CSE-AgNPs. The ACTH2 cells (1×10^6 cells/mL) were treated with 28 and 50 µg/mL of the CSE-AgNPs. Then, the cells were incubated at 37 °C overnight. Afterwards, the cells were harvested by trypsinization, centrifuged and washed twice by PBS. An aliquot of 10 µg/mL fluorescent dyes containing acridine orange/propidium iodide (AO/PI) was added to each well at 25 °C. After 3–5 min, the freshly stained cell suspensions were dropped into a glass slide. Finally, the slides were observed by a fluorescence microscope (Olympus CKX41, Tokyo, Japan). No less than 100 cells were enumerated and the ratio of apoptotic cells was calculated using the following equation [58]:

$$\text{Percentage of total apoptosis cells}(\%) = \frac{\text{Total number of apoptosis cells}}{\text{Total number of apoptosis and normal cells}} \times 100$$

2.5.5. Gene expression assessment

The real-time PCR procedure was applied to compare the expression ranks of BCL2, BAX, Caspase 3, Caspase 9, P53 and HSPA2 gene expression in the untreated cells and the CSE-AgNPs-treated NTERA-2 cells. To this end, NTERA-2 cells were seeded in the cell culture flasks and treated with the CSE-AgNPs at an inhibitory concentration (6 µg/mL) for 24 h.

Total RNA was extracted as a sample using a High Pure RNA isolation kit (Qiagen, Germany). Complementary DAN (cDNA) was synthesized using oligo (dT) and a first-strand complementary fabrication kit based on the manufacturer's guideline (Fermentas, Lithuania). The sequences of the primers and conditions employed in this study are presented in Table 1. The PCR amplification conditions comprised 10 min at 95ºC, followed by 45 cycles of a denaturation phase at 95ºC for 10 min, and annealing and extension for 30 s at 72ºC. The relative gene expression rank was evaluated with the comparative Ct method ($2^{-\Delta\Delta Ct}$). The housekeeping glyceraldehyde-3-phosphate dehydrogenase (*GAPDH*) gene was employed as an internal control [59].

2.6. Statistical analysis

Statistical analysis was performed in SPSS 22 and the results were analyzed by one-way analysis of variance (ANOVA). The expression ranks of the selected genes between the treated samples and the control group were examined using Tukey's HSD post-hoc test. The data were shown as the mean ± standard deviation and $P < 0.05$ was regarded as statistically significant.

3. Results and discussion

3.1. Plant-mediated synthesis of NPs

Stable AgNPs cannot be produced under acidic or neutral solutions; so, AgNPs are synthesized in alkaline media [60]. It is defined as the mechanism of plant-assisted silver nanoparticles based on the following hypothesis. (a) electrostatic interactions was performed between silver ions and biochemically active groups of plant extract; (b) then, silver ions were bio-reduced into silver nuclei, which subsequently grew [61].

It is known that C. *sinensis* contains various polyphenolic compounds, is easily removed from the body in alkaline conditions and acts as a reducing/stabilizing factor [62]. The reduction of silver ions from Ag (I) to Ag (0) in the $AgNO_3$ solution was performed by *C. sinensis* extract and the formation of CSE-AgNPs was indicated by the immediate color change from green to dark brown (Fig. 1A).

The synthesis of the extract-stabilized AgNPs was also verified by UV–Vis spectroscopy, wherein the CSE-AgNPs showed an SPR (surface plasmon resonance) peak at 440–450 nm (Fig. 1B). Comparison of the absorption spectrum obtained from the aqueous extract of *C. sinensis* with the solution containing biosynthesized silver nanoparticles showed that the extract was not absorbed in the corresponding wavelength and

Table 1
The primers sequence and applied conditions for real-time PCR.

Gene name	Forward Primer	Reverse Primer	Annealing temperature	Product size (bp)
BCL2	5′ CAGGATAACGGAGGCTGGGATG 3′	5′ GACTTCACTTGTGGCCCAGAT 3′	59	157
BAX	5′ CCCTTTTGCTTCAGGGTTTCAT 3′	5′ TCAGCTGCCACTCGGAAAAA 3′	59	223
CASPASE3	5′ ACTGGACTGTGGCATTGAG 3′	GAGCCATCCTTTGAATTTCGC 3′ 5′	60	138
CASPASE9	5′ CGGTGACCCCAGAATTGACC 3′	5′ CCTGCCCGCTCACGTC 3′	61	164
P53	5′ TGCTCAAGACTGGCGCTAAA 3′	5′ CAGTCTGGCTGCCAATCCA 3′	59	157
HSPA2	5′ TTGCAACCCCATCATCAGCA 3′	5′ TTGGCACAAGGACATTTCAAAGA 3′	59	192
GAPDH	5′ GGAAGGTGAAGGTCGGAGTCA 3′	5′ GTCATTGATGGCAACAATATCCACT 3′	58	101

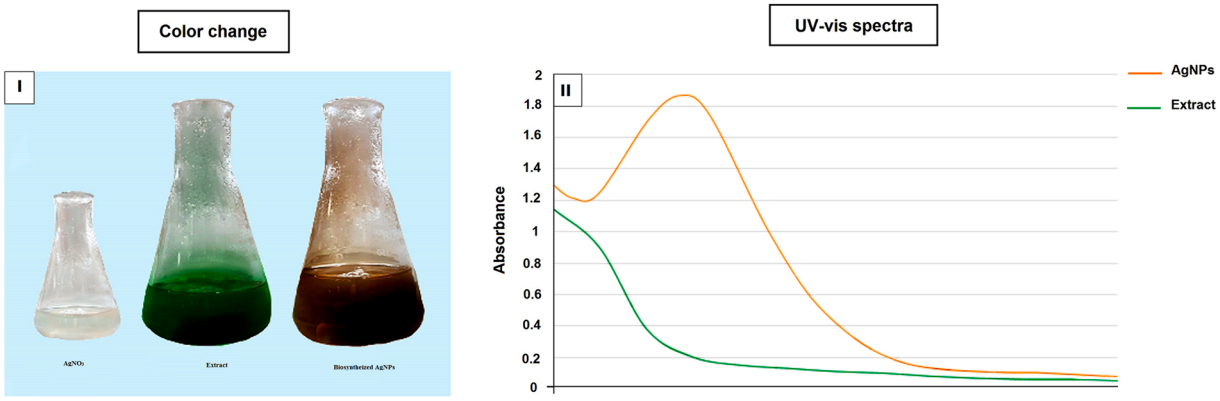

Fig. 1. I) Solutions used in the synthesis of silver nanoparticles using *C. sinensis* extract (CSE-AgNPs). II) UV–Vis spectrophotometry from extract and silver nitrate ($AgNO_3$).

the absorption spectrum observed in the solution was due to the presence of nanoparticles.

3.2. Influence of different parameters on the fabrication of CSE-AgNPs

Initially, 3 mL of the *C. sinensis* extract and 7 mL of the $AgNO_3$ solution were mixed. The color of the colloidal solution turned from green to dark brown and, then, black over time went on, indicating the formation of CSE-AgNPs (Fig. 1A). Different parameters were measured for the synthesis of nanoparticles with the best absorption spectra.

3.2.1. pH optimization

The pH of the resulting solution was estimated at 6 by a pH meter. The effect of pH on the fabrication of NPs was studied at various pH values of 4, 5, 6, 7, 8, 9; the UV–vis spectra of CSE-AgNPs at different pH ranges are depicted in Fig. 2A. An SPR band appeared in the range of 400–450 nm. A sharp and symmetric peak was obtained at pH 8. In the range of pH 4 and 5, there was no suitable absorption peak. At higher pH (pH= 9), the SPR band's position decreased compared to pH 8; so, pH 8 was selected for the synthesis of nanoparticles. Previous studies have shown that the pH reaction did not have a considerable influence on the shape of NPs, but affected the nanoparticle size [63]. At pH= 8, a sharp and symmetrical peak was detected, but at higher pH (pH=9), a decrease in the rate of adsorption was observed; this can suggest Ag-ions were hydrolyzed at the desired acidity, such that the species was formed. The stable hydroxides of silver ions were oxidized and, eventually, prevented from entering the bioremediation reaction [41,64]. With the rise in pH, the SPR bands became broader, which was due to the increased particle size [65]. pH was directly correlated with the steadiness of the NPs. With a rise in pH, the AgNPs with less stability and larger dimensions were created due to CSE-AgNPs aggregation. However, this aggregation was caused by the existence of electrostatic relations between partly ionized sodium citrate groups. At the lower pH, CSE-AgNPs were less aggregated because all groups were protonated, acting toward the electrostatic relations [66]. Therefore, pH 8 was deemed optimal.

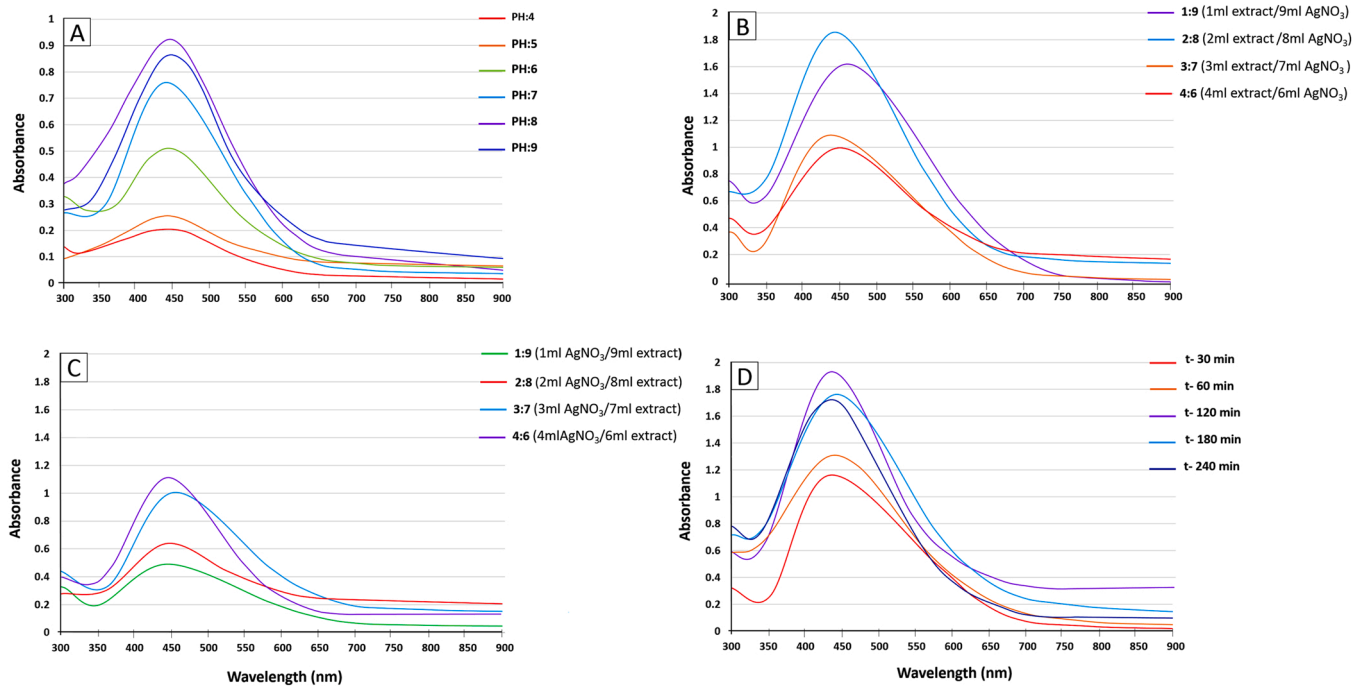

Fig. 2. a) UV–vis spectrophotometry of extract under different pH conditions; b-c) Comparison of absorption spectra at various ratios of extract and silver nitrate ($AgNO_3$); d) Different times efficacy in the synthesis of silver nanoparticles using *C. sinensis* extract (CSE-AgNPs).

3.2.2. Optimization with different concentration ratios

Different concentration ratios of the plant extract and silver nitrate solution at pH 8 were measured. The maximum absorption peak of CSE-AgNPs occurred at the concentration ratio of 2:8 (2 mL extract /8 mL $AgNO_3$), which was further validated by creating the highest peak in UV–Visible spectrophotometry. Thus, this ratio was deemed optimal and the next factor was assessed based on this ratio (Fig. 2B). The intensity of the absorption spectra of CSE-AgNPs rose with increasing the treatment of $AgNO_3$ (6–8 mL). The UV–Vis peak was more prominent for higher $AgNO_3$ treatments than the extract, indicating that more NPs per unit volume was made when $AgNO_3$ concentration was elevated (Fig. 2B, C).

Different studies report that, in biosynthesis, extra Ag-ion concentration is necessary for the better synthesis of AgNPs [67]. Ibrahim et al. reported that when they synthesized AgNPs using $AgNO_3$ as a metal salt and the banana peel extract as a reducing and coating agent, the color changed from yellowish to darker shades of reddish-brown by elevating the concentration of $AgNO_3$ [68]. However, at a higher concentration (9 mL), CSE-AgNPs started to aggregate and form into large particles. Zhang et al. believed that aggregation and formation of large particles were due to two probable bases. Firstly, the creation level of nuclei increased more significantly than the growth degree of Ag-nanocrystals by increasing the $AgNO_3$ content. Secondly, many AgNPs were shaped at higher treatment of $AgNO_3$. Therefore, the collision frequency was enhanced considerably, which resulted in the aggregation of the nanoparticles [69–71]. The current study concluded that the optimum ratio of 2:8 extract/$AgNO_3$ was suitable for AgNPs synthesis.

3.2.3. Optimization of CSE-AgNPs in different reaction times

The interaction time, also known as the reaction time, is a key factor for nanoparticle synthesis. The optimum time results in higher concentrations of CSE-AgNPs in the medium, observed by high absorbance peaks. At different predetermined reaction times (30, 60, 120, 180 and 240 min), a sample was withdrawn and the presence of CSE-AgNPs was recorded by the spectrophotometer. The time, beyond which no further increase in the absorption was observed, was deemed as the completion time of the reaction. A rise in absorbance was detected when the rate of CSE-AgNPs synthesis was enhanced and more particles were shaped at the same time. The plasmon severity at the reaction time of 120 min was close to that at 180 and 240 min, indicating the completion of the reaction. Therefore, the optimum time for the synthesis of CSE-AgNPs was chosen to be 120 min (Fig. 2D). Recent studies have demonstrated that, besides the nature of the plant extracts and types of biologically active molecules, several factors such as pH, concentrations and reaction time can affect the reduction process [72].

3.3. Characteristic of CSE-AgNPs

3.3.1. FTIR spectroscopy study

The FTIR analysis was performed to evaluate the chemical and molecule structures of the plant extract and CSE-AgNPs (Fig. 3). Bio-functional classes linked to the surface of NPs and chemical residues were identified by FTIR; this indicated the possible existence of molecules in the plant extract which were responsible for the Ag-ions' reducing factor. Examining the FTIR spectrum of the *C. sinensis* extract displayed the existence of several biomolecules such as flavonoids and terpenoids [73]. The presence of a broad peak (3441) in the spectrum was associated with the stretching vibrations of O–H hydroxyflavones and catechin groups. The peaks at 2903 cm^{-1} and 1050 cm^{-1} corresponded to the tensile vibrations of the C–H groups. A strong absorption peak at 1635 cm^{-1}, related to tensile vibrations of the C = O bond, indicated a stretch of the acid groups present in the thearubigins. Moreover, the spectra showed a C–O peak at 1256 cm^{-1} and peaks at 826 cm^{-1} and 568 cm^{-1}, confirming the existence of aromatic replaced rings. Apart from a minor shift in the C═O stretch from 1635 cm^{-1} to 1256 cm^{-1}, the rest of the peaks remained unaffected in the spectra based on the CSE-AgNPs after the reaction with the *C. sinensis* extract, as presented in Fig. 3, verifying that CSE-AgNPs were protected by the natural compound known as thearubigins present in the extract [62]. The FT-IR spectra demonstrated the biofunctional classes of molecules existing in the green tea extract that may be accountable for reducing metallic ions and stabilizing AgNPs [74].

3.3.2. XRD examination

The crystalline construction of CSE-AgNPs was determined by the XRD technique [75] (Fig. 4). The fairly wide XRD form displayed the synthesis of AgNPs. The size of CSE-AgNPs was calculated by Debye--Scherrer's formula:

$$\mathbf{D} = \frac{Ky}{\beta \cos f_0(\theta)}$$

where D is the particle dimension, K is a grain sharp factor (0.94), λ is the incident X-ray wavelength (1.5418 Å), β is the full width at half maximum of the deflection peak and θ is Bragg's angle of the peak.

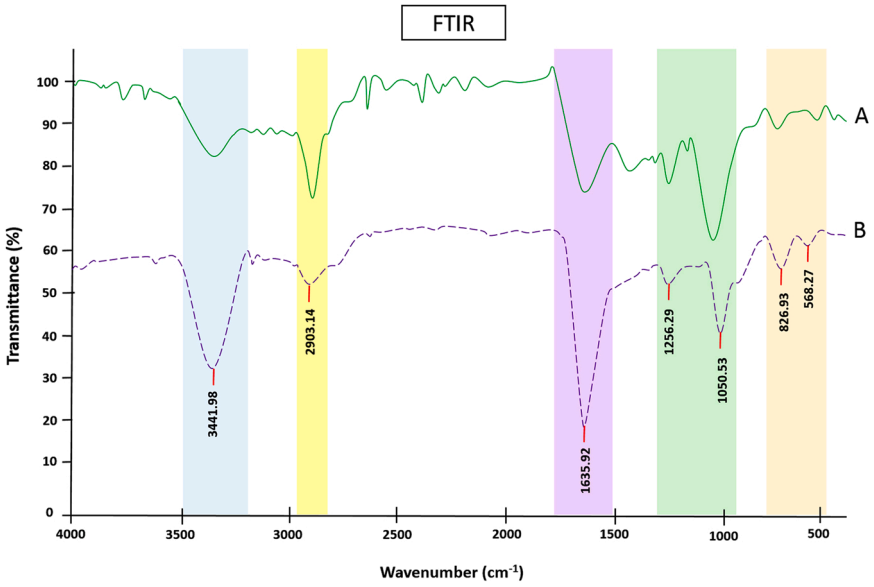

Fig. 3. Fourier transform infrared spectroscopy (FTIR) spectra of (A) extract; (B) biosynthesized silver nanoparticles using *C. sinensis* extract (CSE-AgNPs).

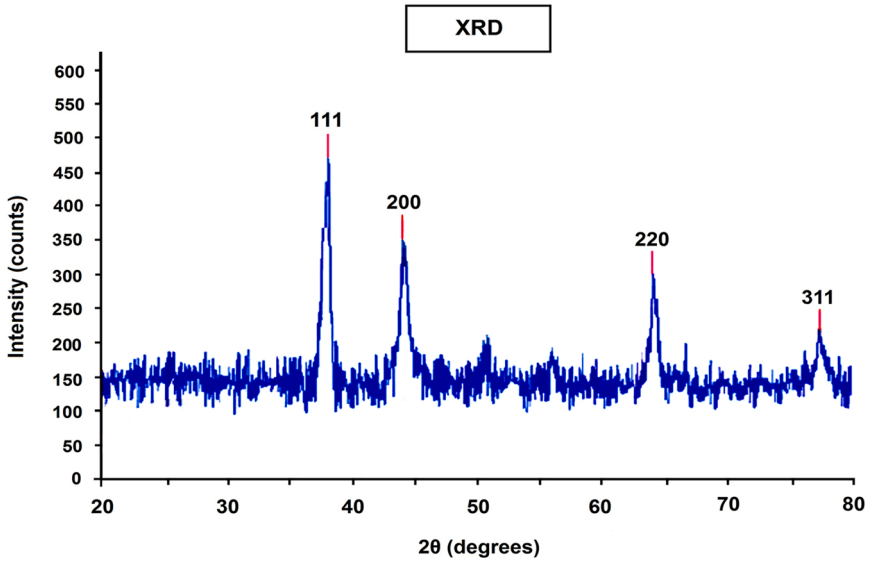

Fig. 4. X-ray diffraction (XRD) pattern of biosynthesized silver nanoparticles using *C. sinensis* extract (CSE-AgNPs). The XRD peaks are placed at angles of 38.16°, 38°, 44°, 64° and 77° matching the 111, 200, 220 and 311 planes of CSE-AgNPs.

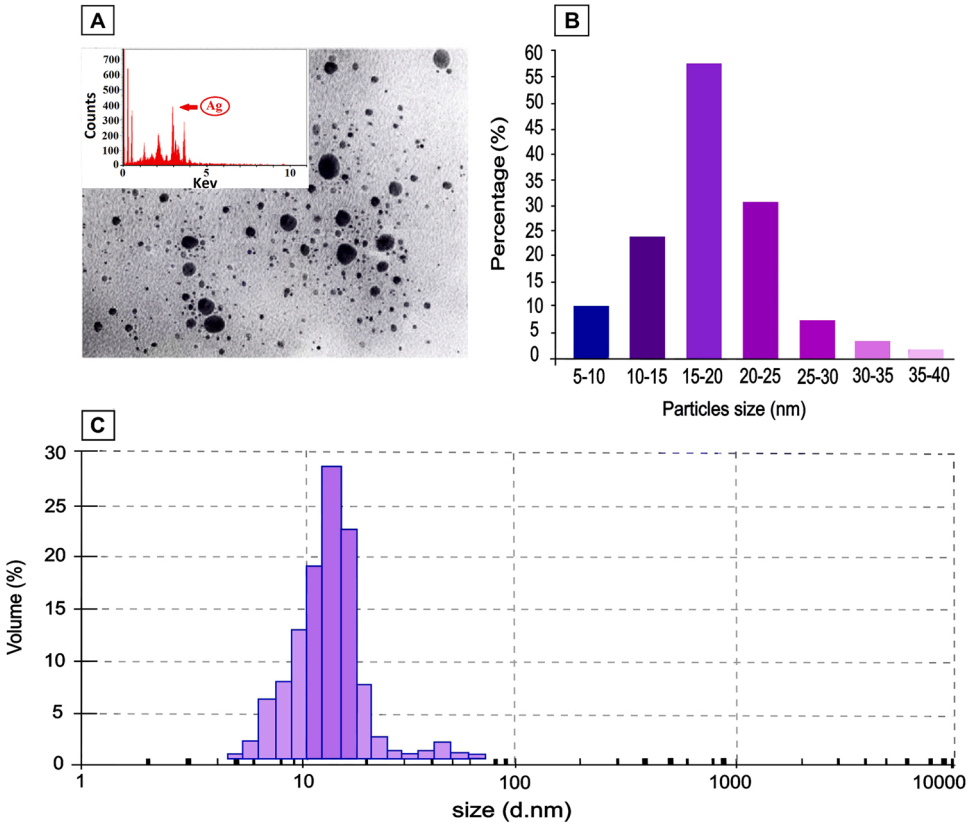

Fig. 5. (A, B) Transmission electron micrograph, energy dispersive spectroscopy (EDS) result of biosynthesized silver nanoparticles using *C. sinensis* extract (CSE-AgNPs) and the pictogram of particle size distribution; (C) Dynamic light scattering (DLS) analysis of CSE-AgNPs.

Prominent peaks at 38, 44, 64° and 77° could be attributed to the (111), (200), (220) and (311) reflection designs, respectively. The peak related to the (111) plane was stronger and sharper than others [55,76]. These results were compatible with the standard deflection data stated for Ag by the JCPDS database (no. 04–0784) [67].

3.3.3. TEM and DLS analysis

DLS and TEM procedures were employed to evaluate the dimension and shape of the CSE-AgNPs (Fig. 5A-C). The TEM showed that the nanoparticles were well-dispersed and had a sphere shape with size varying from 5 to 40 nm. The shape stability of CSE-AgNPs is critical in nanotechnology because shape affects the physicochemical properties of NPs [77]. The morphological characteristics of CSE-AgNPs are

illustrated in Fig. 5A, B. DLS studies were performed for particle size distribution and to obtain the average hydrodynamic diameter of the CSE-AgNPs. The particle size was 8–68 nm in the DLS analysis. The dimension and shape of CSE-AgNPs wen shown to depend on the green tea extract used for fabrication [78]. The EDX test result displayed a sharp signal in the Ag area while affirming that the AgNPs have formed. Due to SPR, normally AgNPs display a characteristic absorption peak at ~3 keV [79].

3.4. Antioxidant activity of biosynthesized silver nanoparticles (CSE-AgNPs)

Free radicals, particularly their enhanced production, have gained momentum in many diseases, including cancer and cardiovascular diseases [80]. The most frequently used methods for determining antioxidant capacities include the ABTS and DPPH radical scavenging assays, while rutin is used as a standard [81]. The results indicate that CSE-AgNPs have a comparable antioxidant activity with the standard antioxidants rutin, while the plant extract exhibited a lower antioxidant activity. CSE-AgNPs showed a notable dose-dependent scavenging property toward all the free radicals (Fig. 6). Researchers have reported that biochemical groups of plant extract involved in the reduction of Ag ions for AgNPs creation can explain their antioxidant properties [82]. The DPPH free radical assay was considered for defining the free radical scavenging property of the fabricated NPs and natural products due to its high stability [83]. DPPH showed a maximum absorption band at 490 nm and was gradually reduced as the antioxidant properties diminished [84]. In this research, DPPH scavenging property rose with an increment in the treatment of the fabricated CSE-AgNPs with the maximum activity of 80.91% at the maximum concentration (100 μg/mL), which was close to that exhibited by the rutin standard in the similar treatment (93.21%); however, the herbal extract displayed noticeably less scavenging property (50.19%), which confirmed that CSE-AgNPs had a high antioxidant potential (Fig. 6A). CSE-AgNPs revealed maximum ABTS+ scavenging property (92.16%), almost equivalent to that displayed by the rutin standard (95.44%) at 100 μg/mL, demonstrating a strong property. The results were in agreement with those of Shanmugam et al., showing that the ABTS+ scavenging property of biosynthesized AgNPs is strong [85] (Fig. 6B). In the present study, the CSE-AgNPs fabricated via a green procedure displayed high antioxidant properties, consistent with the results of Selvan et al. [55].

The results of the current study were confirmed by Magdy et al. who reported similar outcomes when working with AgNPs modified by green tea extract [86]. Additionally, Magdy et al. stated that the antioxidant activity of the plant extract may be a highly probable mechanism that helps prevent AgNPs' toxicity. They reported that green tea extract can not only mitigate the side effects of AgNPs, but has anti-cancer effects against Ehrlich ascitic carcinoma; therefore, it can be useful in the treatment of AgNPs-related liver dysfunction [86]. Further molecular research is required to fill in this scientific gap. The IC50 value of CSE-AgNPs, the extract and relevant standards for all the considered antioxidants are presented in Table 2. Herein, the CSE-AgNPs displayed maximum properties toward DPPH scavenging activity with the IC50 of 8.78 μg/mL, whereas the minimum activity was toward ABTS+ cation radical with the IC50 of 9.82 μg/mL. Compared to rutin as a standard, the antioxidant activity of CSE-AgNPs increased more significantly than the *C. sinensis* extract.

Table 2
The IC50 value of biosynthesized silver nanoparticles using *C. sinensis* extract (CSE-AgNPs), an extract compared to Rutin as a standard.

	IC50 (μg/mL)		
	Rutin	Silver nanoparticles	Plant extract
ABTS	4.36	9.82	24.9
DPPH	3.26	8.78	98.7

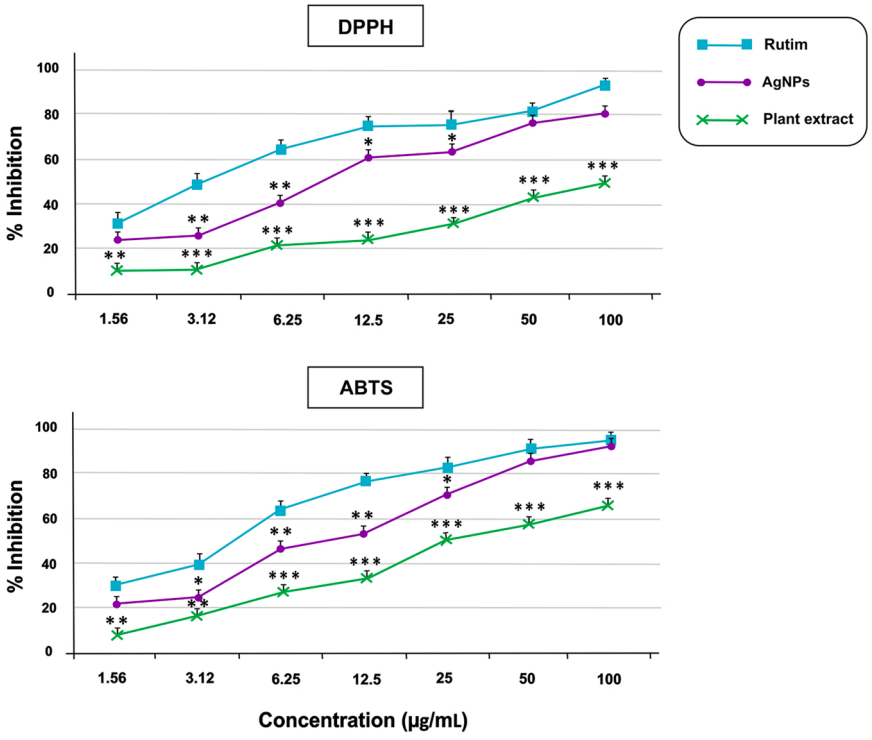

Fig. 6. Antioxidant scavenging properties of extract and biosynthesized silver nanoparticles using *C. sinensis* extract (CSE-AgNPs). (A) 2,2-diphenyl-1-picrylhydrazyl (DPPH) radical scavenging action, (B) 2,2′-azino-bis(3-ethylbenzothiazoline-6-sulfonic acid (ABTS) scavenging action. Values are mean ± SD of triplicate examinations (n = 3). Significant changes are denoted by $*p < 0.05$, $**p < 0.01$ and $***p < 0.001$ versus control (rutin).

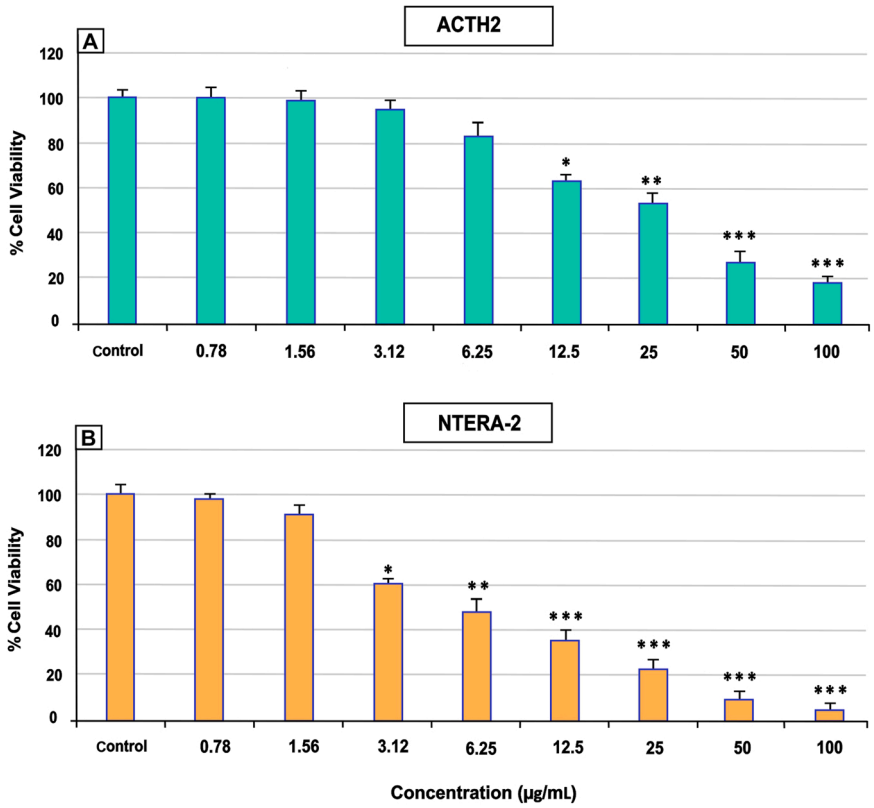

Fig. 7. The mean percentage of normal human testis (ACTH2) and cancerous cells (NTERA-2) proliferation in cells treated with various concentrations of biosynthesized silver nanoparticles using *C. sinensis* extract (CSE-AgNPs) performed by 3-[4,5-dimethylthiazole-2-yl]-2,5-diphenyltetrazolium bromide (MTT) assay in 24 h. Error bars represent the mean±SD of triplicate analyses (n = 3). Significant changes are shown by $*p < 0.05$, $**p < 0.01$ and $***p < 0.001$.

3.5. *In vitro cytocompatibility of CSE-AgNPs*

MTT assay was performed to measure the influence of CSE-AgNPs on the survival and proliferation of NTERA-2 and ACTH2 cell lines. Various concentrations of CSE-AgNPs (0, 0.78, 1.56, 3.12, 6.25, 12.5, 25 50, and 100 µg/mL) were evaluated in both cell lines after 24 h (Fig. 7). In the NTERA-2 cell line, there was no noteworthy change in cell proliferation between CSE-AgNPs-treated cells (0.78, 1.56 µg/mL concentrations) and untreated cells (control). The cell proliferation was significantly decreased in the presence of 3.12 µg/mL of CSE-AgNPs compared to the control cells ($p < 0.05$). The cell proliferation was significantly reduced in 6.25 µg/mL of CSE-AgNPs compared to the control cells ($p < 0.01$). The cell proliferation in the treated cells with high treatments of CSE-AgNPs (12.5, 25, 50, 100 µg/mL) was significantly lower than the control cells ($p < 0.001$). In the ACTH2 cell line, there was no substantial change in the bioavailability percentage of 0.78, 1.56, 3.12 and 6.25 µg/mL of CSE-AgNPs compared to the control group. At 12.5 µg/mL and 25 µg/mL concentrations, CSE-AgNPs showed a significant reduction in the treated cells compared to the control group (respectively at $p < 0.05$ and $p < 0.01$). The maximum inhibitory effect was observed on ACTH2 cell propagation at 100 µg/mL, which was statistically significant compared to the control cells ($p < 0.001$).

There was an inverse relationship between the dosage of NPs and cell viability; as the concentration of CSE-AgNPs increased, the cell proliferation decreased. AgNPs may induce reactive oxygen species (ROS), the activity of which on cells leads to cellular death [87]. It has been reported that cancer cell line viability decreases with increasing the concentrations of AgNPs [88]. According to the results of these experiments, the IC50 of CSE-AgNPs on ACTH2 cell line viability was 28 µg/mL after 24 h of incubation. (Fig. 7A). The IC50 value was 6 µg/mL for CSE-AgNPs against the NTERA-2 cells in 24 h, which was lower than the IC50 for the ACTH2 cells (Fig. 7B). The results indicated that a lower treatment of CSE-AgNPs is necessary to prevent 50% of the NTERA-2 cell line. These results confirmed that cancer cells are more sensitive than normal cells to exposure to CSE-AgNPs. The findings of this study are consistent with the results of Selvan et al., which showed that the biosynthesized AgNPs had the highest cytotoxicity activity against cancer cells compared to normal cells [55]. The results of the present study suggested that biosynthesized AgNPs reduced the viability of cells in a dose-dependent manner. Most of the cells uptake AgNPs through endocytosis [89]. Internalized AgNPs can be found in mitochondria and the nucleus [90]. Once internalized, intracellular AgNPs induce a series of effects including oxidative stress, cell cycle rest, impairment of the cell membrane, inflammatory responses, DNA damage and genotoxicity, chromosome aberrations and apoptosis [91–93]. The AgNP exposure could induce the changes of cell shape, reduce cell viability, increase lactate dehydrogenase (LDH) release and, finally, result in cell apoptosis and necrosis [46,92,93]. In addition, damage to mitochondria disrupts electron transfer inhibits the synthesis of adenosine triphosphate (ATP), stimulates oxidative stress and activates mitochondrial apoptosis [91].

3.6. *Cell population changes by AO/PI staining*

Apoptosis was evaluated by staining NTERA-2 and ACTH2 cells with acridine orange/ propidium iodide (AO/PI). This assay was performed on non-treated cells as the control, treated cells with the IC50 concentration and treated cells with higher than IC50 concentrations of CSE-AgNPs. The AO/PI fluorescence microscopic staining was performed to observe the morphological alterations in NTERA-2 and ACTH2 cells. Viable cells appeared as green; early- and late-apoptotic cells as green-orange and dark orange, respectively. Necrotic cells appeared brown and reddish-brown (Fig. 8A-F). The ACTH2 cells were treated with 0 µg/mL, 28 µg/mL (IC50) and 50 µg/mL concentrations of CSE-AgNPs. At the 28 µg/mL and 50 µg/mL, the percentage of dead cells was detected

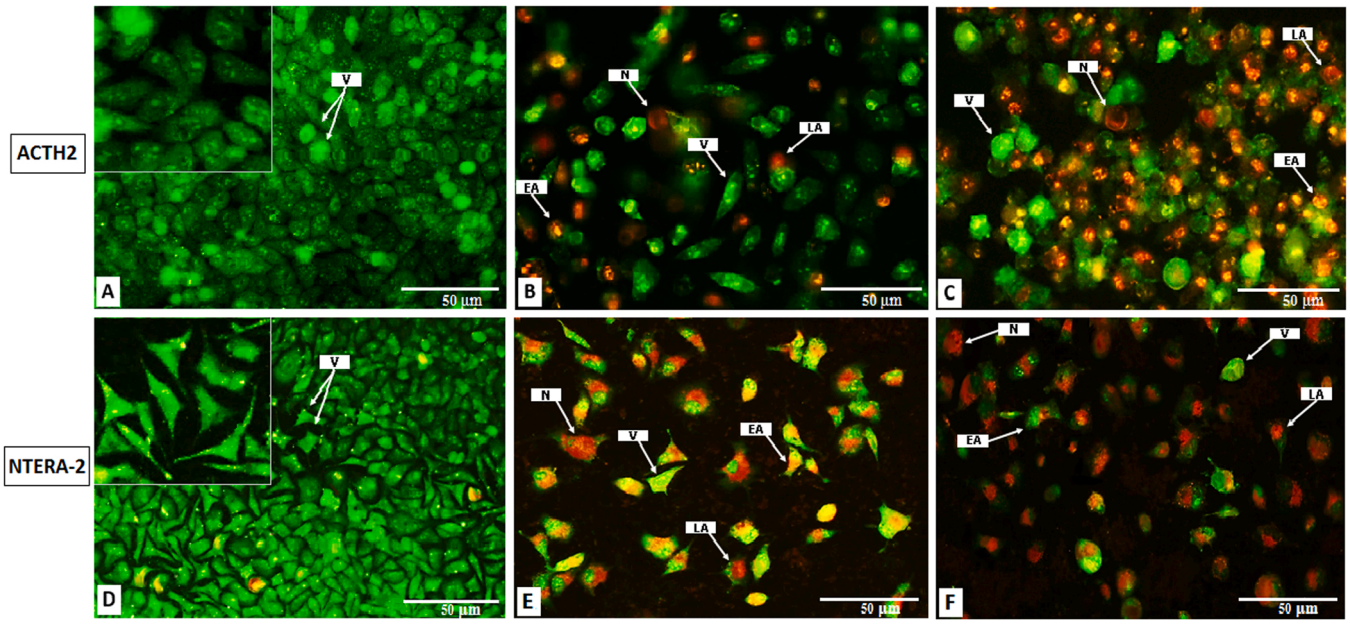

Fig. 8. Morphological observation of normal human testis (ACTH2) and cancerous cells (NTERA-2) treated with the extract and biosynthesized silver nanoparticles using *C. sinensis* extract (CSE-AgNPs) by AO/PI staining. ACTH2 cells were treated with A) 0, B) 28 and C) 50 µg/mL of CSE-AgNPs. NTERA-2 cells were treated with A) 0, B) 6 and C) 12.5 µg/mL of CSE-AgNPs. (A, D): Untreated cells (control) appeared mostly as homogenously green and normal constructions with very little apoptosis and necrosis. Treated cells at concentrations of 28, 50, 6 and 12.5 µg/mL of CSE-AgNPs (B, C, E and F), revealed initial and late apoptosis and necrosis. Early apoptosis morphologies were orange-green amongst the chromatin condensation and fragmented DNA. Late apoptosis appeared as dark orange and bright red necrosis. Cells were presented as viable (V), late-apoptotic (LA), early-apoptotic (EA) and necrotic (N). The values are displayed as mean±SD. (200× and 400× magnification).

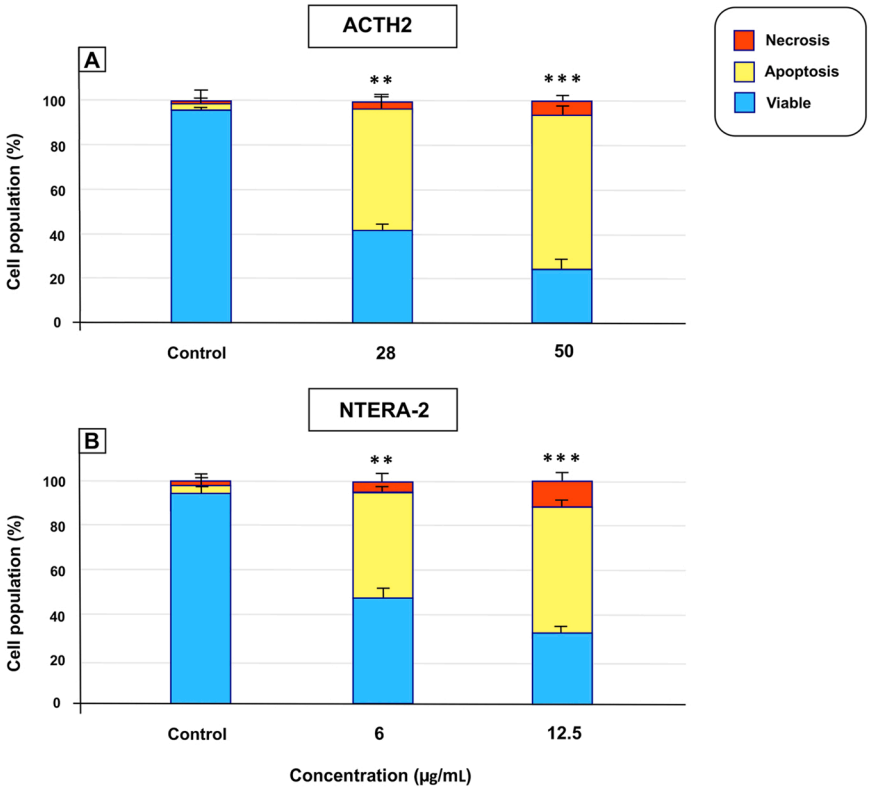

Fig. 9. Calculation of viable, apoptotic and necrotic percentages of normal human testis (ACTH2) and Cancer cells (NTERA-2) treated with different concentrations of biosynthesized silver nanoparticles using *C. sinensis* extract (CSE-AgNPs) (A-B) by AO/PI staining. ACTH2 cells were treated with concentrations of 0, 28 and 50 µg/mL of biosynthesized silver nanoparticles using *C. sinensis* extract (CSE-AgNPs). NTERA-2 were treated with concentrations of 0, 6 and 12.5 µg/mL of AgNPs compared with the control group (** $p < 0.01$, ***$p < 0.001$).

as 58% and 76%, respectively ($p < 0.01$, $p < 0.001$) (Fig. 9A). Moreover, the percentage of the apoptotic and necrotic cells at the 50 µg/mL concentration increased by 24% and 4%, respectively, compared to the cells treated with 28 µg/mL of CSE-AgNPs. In addition, in the NTERA-2 cells, > 90% of the cells were viable in the controls, while 53% and 68% of the treated cells were dead at the 6 µg/mL (IC50) and 12 µg/mL concentrations of CSE-AgNPs (respectively at $p < 0.01$ and $p < 0.001$) (Fig. 9B). The graph of the cell population revealed that, in the CSE-

AgNPs-treated cells with 12 μg/mL, the number of apoptotic cells increased by 13% and the number of necrotic cells was enhanced by 8% compared to 6 μg/mL of CSE-AgNPs. The results of AO/PI staining indicated that treatment with the IC50 concentrations of CSE-AgNPs in cancer cells (NTERA-2) caused more apoptosis than the normal cells (ACTH2) (Fig. 9B). In this regard, the AO/PI results are consistent with previous studies using the MTT assay. It has been shown that cell death induced by AgNPs through apoptosis and necrosis demonstrates characteristic nuclear alterations, e.g., chromatin condensation and nuclear destruction, in the cells [94,95].

In fact, CSE-AgNPs-treated cells, especially at higher concentrations than IC50, showed clear fragmented DNA ladders, suggesting that cell death is due to apoptosis. In general, the fragmented DNA indicates apoptotic process [96]. Also, some works have demonstrated that caspase 3 activation mediates the apoptotic process [97]. In the present study, AO/PI staining induced apoptosis in CSE-AgNPs-treated NTERA-2 cells at IC50 concentrations and above, which was consistent with the real-time PCR results showing an increase in caspase 3 levels. Therefore, apoptosis-inducing agents, such as biosynthesized silver nanoparticles that specifically target tumor cells at lower concentrations than normal cells and may have the potential to develop as new antitumor drugs, could be a new source for anti-cancer drugs.

3.7. Examining apoptotic gene expression by real-time PCR

Gene expression in NTERA-2 cells exposed to CSE-AgNPs at the IC50 concentration (6 μg/mL) was assessed using real-time PCR after 24 h (Fig. 10). The expression of Bax, Bcl2, caspase 3 and caspase 9 genes that are associated with apoptotic markers and other related genes, p53 and HSPA2 was compared to that of the untreated cells (control). The disruption of an apoptotic pathway can be caused by alterations in the cell number homeostasis, which leads to the development of cancer [98,99]. Pro-apoptotic protein Bax and anti-apoptotic protein Bcl-2 strictly control the balance between the cell life and death [100,101]. Bcl-2 protects the cells against apoptosis by connecting to Bax, stimulates permeability transition, prevents them from translocation to mitochondria and oligomerization, and subsequently, activates caspase cascade [102]. However, the gene expression of Bax and Bcl2 as well as the subsequent downstream activation of caspase protein indicated the stimulation of mitochondrial apoptosis in cancer cell lines [103]. Herein, an increment in the mRNA ranks of caspase 3 and caspase 9 genes at the IC50 concentration of CSE-AgNPs was observed (2.23- and 1.42-fold change; $p < 0.001$, $p < 0.05$, respectively) in NTERA-2 cells compared to the control group. Moreover, the mRNA level of Bax was significantly upregulated (2.71-fold change, $p < 0.001$), while the gene expression of Bcl-2 was significantly reduced (1.24-fold change, $p < 0.01$) in the treated cells compared to control cells. These results confirm that the exposure of CSE-AgNPs induced substantial apoptosis in NTERA-2 cells. Mousavi et al. produced biosynthesis nanoparticles with the mean diameter of 21.22 nm, which was similar to the particle size of NPs in this current research. They also reported that AgNPs increased apoptosis in the treated cells compared to the control ones [104]. In a recent study, the significant upregulation of caspase 3 and caspase 9 genes in human ovarian cancer cells (PA-1 cell line) treated with biosynthesis nanoparticles confirmed that apoptosis probably occurred in a caspase family-mediated manner [105].

The tumor suppressor gene P53 (tumor protein p53) acts as an anti-cancer gene by activating cell death through apoptosis, as well as stopping the cell cycle in cancer cells. P53-induced apoptosis is mediated by apoptosis-relating proteins. The p53 induces apoptosis by regulating the transcription of the pro-apoptotic members of the Bcl2 family and releasing cytochrome-c as of mitochondria through its mitochondrial translocation [106,107]. However, p53 is the most regularly deactivated gene and is often mutated in hominid cancerous cells. The p53 pathway may explain the impaired tumor suppressor function, drug resistance and weak chemotherapeutic outcomes [108]. The results showed significantly higher expression of p53 mRNA level (2.33-fold change, $p < 0.001$) (Fig. 10). It has been demonstrated that p53 mRNA expression is associated with Bax mRNA expression, while the caspase 9 mRNA expression pre-treatment is not associated with Bax and p53 mRNA expression [109].

Heat shock proteins (HSP) are vital proteins, noticeably expressed in reaction to oxidative stress, chemicals and heat [110]. These proteins are chiefly involved in protein assemblage, folding, transport and targeting for lysosome deprivation [111]. HSPA2 (heat shock-related 70 kDa protein 2) has been associated with the cancer-enhancing protein expressed at irregular ranks in a subdivision of cancers [112]. The expression of HSPA2 mRNA in NTERA-2 cells treated with CSE-AgNPs was significantly increased (1.65-fold change, $p < 0.01$) in comparison to control cells. Jagadish et al. reported that HSP70–2 was over-expressed in breast cancer patients and reduced tumor growth [112]. The results hinted that CSE-AgNPs can significantly increase the

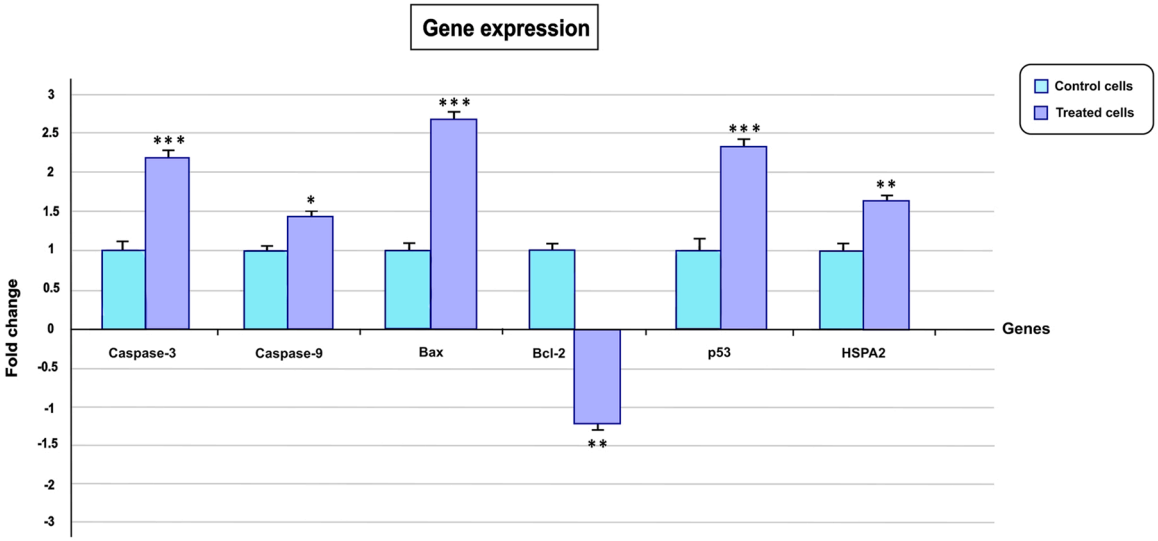

Fig. 10. Real-time PCR examination for Bax, Bcl2, caspase 3, caspase 9, p53 and HSPA2 *mRNA* expression at the IC50 dose of biosynthesized silver nanoparticles using *C. sinensis* extract (CSE-AgNPs) in cancer cells (NTERA-2) and control cells in 24 h. Significant changes are denoted by $*p < 0.05$, $**p < 0.01$ and $***p < 0.001$ versus control.

expression of Bax, caspase 3, caspase 9, p53 and HSPA2 genes, are associated with apoptotic markers through the change in mitochondrial membrane permeability and are used as a therapeutic agent for testicular cancer cells.

4. Conclusions

Nanoparticles have been widely utilized as an efficient therapy thanks to their beneficial properties. Recently, the biological synthesis of nanoparticles with plants, fungi and bacteria has gained popularity. These natural resources act as reducing/capping factors and affect the attributes and performance of NPs for different applications. AgNPs obtained by the biosynthetic method are cost-effective, biocompatible, pollutant-free and easy to produce. In the present report, AgNPs were synthesized using the green tea (*C. sinensis*) extract (CSE-AgNPs). Preparation of CSE-AgNPs was optimized by different parameters and, eventually, pH of 8, ratio of 2:8 (2 mL plant extract /8 mL $AgNO_3$ solution) and reaction time of 120 min were selected as optimum parameters. Characterization of the optimized CSE-AgNPs confirmed the spherical shape of the AgNPs with dimensions in the range of 5–40 nm. Herein, the CSE-AgNPs had more antiproliferative effects on NTERA-2 cells than ACTH2 cells at the half inhibitory concentration (IC50) of nanoparticles and promoted apoptosis in cancer cells dose-dependently. These nanoparticles also affected the expression of apoptotic indicators (i.e., Bax, Bcl2, caspase 3 and caspase 9). CSE-AgNPs induced apoptosis through the P53-dependent apoptotic pathway in cancer cells. HSPA2 was also involved in the apoptosis process on the cells exposed to CSE-AgNPs. The present study proved the application of synthesized nanoparticles in the treatment of testicular cancer due to its high antioxidant properties, high toxicity against cancer cells and safety against normal cells. Thus, the fabricated CSE-AgNPs may be considered as a promising treatment strategy for testicular cancer. Future studies can focus on the cell and molecular mechanism of the CSE-AgNPs in vivo and fill in this research gap. Studies can also assess the properties and applications of CSE-AgNPs in the treatment of several cancers.

Declaration of Competing Interest

The authors declare that they have no known competing financial interests or personal relationships that could have appeared to influence the work reported in this paper.

Acknowledgments

The authors are grateful to Mashhad University of Medical Sciences and Omid Cancer Center for their financial provision (Grant number: 971060).

References

[1] M. Ashna, A. Es-Haghi, M. Karimi Noghondar, D. Al Amara, M.E.T. Yazdi, Greener synthesis of cerium oxide nanoemulsion using pollen grains of Brassica napus and evaluation of its antitumour and cytotoxicity properties, Mater. Technol. (2020) 1–8.
[2] A. Rauf, T.A. Tabish, I.M. Ibrahim, M.R. ul Hassan, S. Tahseen, M.A. Sandhu, G. Shahnaz, A. Rahdar, M. Cucchiarini, S. Pandey, Design of mannose-coated rifampicin nanoparticles modulating the immune response and Rifampicin induced hepatotoxicity with improved oral drug delivery, Arab. J. Chem. 14 (9) (2021), 103321.
[3] K. Govindaraju, R. Vasantharaja, K.U. Suganya, S. Anbarasu, K. Revathy, A. Pugazhendhi, D. Karthickeyan, G. Singaravelu, Unveiling the anticancer and antimycobacterial potentials of bioengineered gold nanoparticles, Process Biochem. 96 (2020) 213–219.
[4] I. Ali, Nano anti-cancer drugs: pros and cons and future perspectives, Curr. Cancer Drug Targets 11 (2) (2011) 131–134.
[5] I. Ali, K. Saleem, D. Wesselinova, A. Haque, Synthesis, DNA binding, hemolytic, and anti-cancer assays of curcumin I-based ligands and their ruthenium (III) complexes, Med. Chem. Res. 22 (3) (2013) 1386–1398.
[6] I. Ali, W.A. Wani, A. Haque, K. Saleem, Glutamic acid and its derivatives: candidates for rational design of anticancer drugs, Future Med. Chem. 5 (8) (2013) 961–978.
[7] A. Es-haghi, M.E. Taghavizadeh Yazdi, M. Sharifalhoseini, M. Baghani, E. Yousefi, A. Rahdar, F. Baino, Application of response surface methodology for optimizing the therapeutic activity of ZnO nanoparticles biosynthesized from Aspergillus niger, Biomimetics 6 (2) (2021) 34.
[8] V.S. Sivasankarapillai, A.K. Somakumar, J. Joseph, S. Nikazar, A. Rahdar, G. Z. Kyzas, Cancer theranostic applications of MXene nanomaterials: recent updates, Nano-Struct. Nano-Objects 22 (2020), 100457.
[9] R. Saravani, S. Sargazi, R. Saravani, M. Rabbani, A. Rahdar, P. Taboada, Newly crocin-coated magnetite nanoparticles induce apoptosis and decrease VEGF expression in breast carcinoma cells, J. Drug Deliv. Sci. Technol. 60 (2020), 101987.
[10] I. Ali, H.Y. Aboul-Enein, A. Ghanem, Enantioselective toxicity and carcinogenesis, Curr. Pharm. Anal. 1 (1) (2005) 109–125.
[11] I. Ali, M.N. Lone, H.Y. Aboul-Enein, Imidazoles as potential anticancer agents, MedChemComm 8 (9) (2017) 1742–1773.
[12] I. Ali, M. Nadeem Lone, Z.A. Al-Othman, A. Al-Warthan, M. Marsin Sanagi, Heterocyclic scaffolds: centrality in anticancer drug development, Curr. Drug Targets 16 (7) (2015) 711–734.
[13] R. Paridaens, L. Biganzoli, P. Bruning, J. Klijn, T. Gamucci, S. Houston, R. Coleman, J. Schachter, A. Van Vreckem, R. Sylvester, Paclitaxel versus doxorubicin as first-line single-agent chemotherapy for metastatic breast cancer: a European Organization for Research and Treatment of Cancer Randomized Study with cross-over, J. Clin. Oncol. 18 (4) (2000), 724-724.
[14] M.S. Al, Aboody, Cytotoxic, antioxidant, and antimicrobial activities of Celery (Apium graveolens L.), Bioinformation 17 (1) (2021) 147–156.
[15] I. Ali, W.A. Wani, K. Saleem, A. Haque, Thalidomide: a banned drug resurged into future anticancer drug, Curr. Drug Ther. 7 (1) (2012) 13–23.
[16] I. Ali, K. Saleem, H.Y. Aboul-Enein, A. Rather, Social aspects of cancer genesis, Cancer Ther. 8 (2011).
[17] I. Ali, W.A. Wani, A. Khan, A. Haque, A. Ahmad, K. Saleem, N. Manzoor, Synthesis and synergistic antifungal activities of a pyrazoline based ligand and its copper (II) and nickel (II) complexes with conventional antifungals, Microb. Pathog. 53 (2) (2012) 66–73.
[18] I. Ali, W.A. Wani, K. Saleem, M.-F. Hsieh, Anticancer metallodrugs of glutamic acid sulphonamides: in silico, DNA binding, hemolysis and anticancer studies, RSC Adv. 4 (56) (2014) 29629–29641.
[19] I. Ali, Nano Drugs: Novel Agents for Cancer Chemo-therapy, 2011, p. 130.
[20] I. Ali, M.N. Lone, Z.A. Alothman, A.Y. Badjah, A.G. Alanazi, Spectroscopic and in silico DNA binding studies on the interaction of some new N-substituted rhodanines with calf-thymus dna: in vitro anticancer activities, Anti-Cancer Agents Med. Chem. (Former. Curr. Med. Chem. Anti-Cancer Agents) 19 (3) (2019) 425–433.
[21] I. Ali, S.D. Mukhtar, M.F. Hsieh, Z.A. Alothman, A. Alwarthan, Facile synthesis of indole heterocyclic compounds based micellar nano anti-cancer drugs, RSC Adv. 8 (66) (2018) 37905–37914.
[22] I. Ali, A. Haque, W.A. Wani, K. Saleem, M. Al Za'abi, Analyses of anticancer drugs by capillary electrophoresis: a review, Biomed. Chromatogr. 27 (10) (2013) 1296–1311.
[23] I. Ali, M. Nadeem Lone, M. Suhail, S. Danish Mukhtar, L. Asnin, Advances in nanocarriers for anticancer drugs delivery, Curr. Med. Chem. 23 (20) (2016) 2159–2187.
[24] M.E.T.Y. Mohammad Sadegh Amiri, Mostafa Rahnama, Medicinal plants and phytotherapy in Iran: glorious history, current status and future prospects, Plant Sci. Today 8 (1) (2021) 95–111.
[25] D.C. Baird, G.J. Meyers, J.S. Hu, Testicular cancer: diagnosis and treatment, Am. Fam. Physician 97 (4) (2018) 261–268.
[26] T. Gil, S. Sideris, F. Aoun, R. Van Velthoven, N. Sirtaine, M. Paesmans, L. Ameye, A. Awada, D. Devriendt, A. Peltier, Testicular germ cell tumor: short and long-term side effects of treatment among survivors, Mol. Clin. Oncol. 5 (3) (2016) 258–264.
[27] M.R. Hashemzadeh, M.E.T. Yazdi, M.S. Amiri, S.H. Mousavi, Stem cell therapy in the heart: biomaterials as a key route, Tissue Cell (2021), 101504.
[28] Z. Shamasi, A. Es-haghi, M.E. Taghavizadeh Yazdi, M.S. Amiri, M. Homayouni-Tabrizi, Role of Rubia tinctorum in the synthesis of zinc oxide nanoparticles and apoptosis induction in breast cancer cell line, Nanomed. J. 8 (1) (2021) 65–72.
[29] R. Tietze, J. Zaloga, H. Unterweger, S. Lyer, R.P. Friedrich, C. Janko, M. Pöttler, S. Dürr, C. Alexiou, Magnetic nanoparticle-based drug delivery for cancer therapy, Biochem. Biophys. Res. Commun. 468 (3) (2015) 463–470.
[30] M.E.T. Yazdi, M.S. Amiri, S. Akbari, M. Sharifalhoseini, F. Nourbakhsh, M. Mashreghi, M.R. Abbasi, M. Modarres, A. Es-haghi, Green synthesis of silver nanoparticles using helichrysum graveolens for biomedical applications and wastewater treatment, BioNanoScience 10 (4) (2020) 1121–1127.
[31] M. Zarei, E. Karimi, E. Oskoueian, A. Es-Haghi, M.E.T. Yazdi, Comparative study on the biological effects of sodium citrate-based and apigenin-based synthesized silver nanoparticles, Nutr. Cancer 73 (8) (2021) 1511–1519.
[32] J. Shao, Y. Fang, R. Zhao, F. Chen, M. Yang, J. Jiang, Z. Chen, X. Yuan, L. Jia, Evolution from small molecule to nano-drug delivery systems: an emerging approach for cancer therapy of ursolic acid, Asian J. Pharm. Sci. (2020).
[33] M. Javad Farhangi, A. Es-haghi, M.E. Taghavizadeh Yazdi, A. Rahdar, F. Baino, MOF-mediated synthesis of CuO/CeO2 composite nanoparticles: characterization and estimation of the cellular toxicity against breast cancer cell line (MCF-7), J. Funct. Biomater. 12 (4) (2021) 53.
[34] V. Mohammadzadeh, M. Barani, M.S. Amiri, M.E.T. Yazdi, M. Hassanisaadi, A. Rahdar, R.S. Varma, Applications of plant-based nanoparticles in nanomedicine: a review, Sustain. Chem. Pharm. 25 (2022), 100606.

[35] M.E.T. Yazdi, J. Khara, M.R. Housaindokht, H.R. Sadeghnia, S.E. Bahabadi, M. S. Amiri, H. Mosawee, D. Taherzadeh, M. Darroudi, Role of Ribes khorassanicum in the biosynthesis of AgNPs and their antibacterial properties, IET Nanobiotechnol. 13 (2) (2018) 189–192.
[36] M.R. Rezaei, A. Es-haghi, P. Yaghmaei, M. Ghobeh, Biological fabrication of Ag/Ag2O nanoparticles by Haplophyllum obtusifolium watery extract: characterisation and estimation of its biochemical activities, Micro Nano Lett. (2020).
[37] S.M. Mousavi-Kouhi, A. Beyk-Khormizi, M.S. Amiri, M. Mashreghi, M.E.T. Yazdi, Silver-zinc oxide nanocomposite: from synthesis to antimicrobial and anticancer properties, Ceram. Int. (2021).
[38] M.E.T. Yazdi, F. Nourbakhsh, M. Mashreghi, S.H. Mousavi, Ultrasound-based synthesis of ZnO·Ag 2 O 3 nanocomposite: characterization and evaluation of its antimicrobial and anticancer properties, Res. Chem. Intermed. 47 (3) (2021) 1285–1296.
[39] D.P. Lankveld, A.G. Oomen, P. Krystek, A. Neigh, A. Troost–de Jong, C. Noorlander, J. Van Eijkeren, R. Geertsma, W. De Jong, The kinetics of the tissue distribution of silver nanoparticles of different sizes, Biomaterials 31 (32) (2010) 8350–8361.
[40] M.E.T. Yazdi, J. Khara, H.R. Sadeghnia, S.E. Bahabadi, M. Darroudi, Biosynthesis, characterization, and antibacterial activity of silver nanoparticles using Rheum turkestanicum shoots extract, Res. Chem. Intermed. 44 (2) (2018) 1325–1334.
[41] M.E. Taghavizadeh Yazdi, A. Hamidi, M.S. Amiri, R. Kazemi Oskuee, H. A. Hosseini, A. Hashemzadeh, M. Darroudi, Eco-friendly and plant-based synthesis of silver nanoparticles using Allium giganteum and investigation of its bactericidal, cytotoxicity, and photocatalytic effects, Mater. Technol. 34 (8) (2019) 490–497.
[42] M.S. Jabir, A.A. Hussien, G.M. Sulaiman, N.Y. Yaseen, Y.H. Dewir, M.S. Alwahibi, D.A. Soliman, H. Rizwana, Green synthesis of silver nanoparticles from Eriobotrya japonica extract: a promising approach against cancer cells proliferation, inflammation, allergic disorders and phagocytosis induction, Artif. Cells Nanomed. Biotechnol. 49 (1) (2021) 48–60.
[43] M. Hassanisaadi, G.H.S. Bonjar, A. Rahdar, S. Pandey, A. Hosseinipour, R. Abdolshahi, Environmentally safe biosynthesis of gold nanoparticles using plant water extracts, Nanomaterials 11 (8) (2021) 2033.
[44] S.M. Mousavi-Kouhi, A. Beyk-Khormizi, V. Mohammadzadeh, M. Ashna, A. Es-haghi, M. Mashreghi, V. Hashemzadeh, H. Mozafarri, M. Nadaf, M. E. Taghavizadeh Yazdi, Biological synthesis and characterization of gold nanoparticles using Verbascum speciosum Schrad. and cytotoxicity properties toward HepG2 cancer cell line, Res. Chem. Intermed. (2021) 1–12.
[45] A. Rahdar, S. Rahdar, G. Labuto, Environmentally friendly synthesis of Fe2O3@SiO2 nanocomposite: characterization and application as an adsorbent to aniline removal from aqueous solution, Environ. Sci. Pollut. Res. (2020) 1–11.
[46] M.E. Taghavizadeh Yazdi, M. Darroudi, M.S. Amiri, H. Zarrinfar, H.A. Hosseini, M. Mashreghi, H. Mozafarri, A. Ghorbani, S.H. Mousavi, Antimycobacterial, anticancer, antioxidant and photocatalytic activity of biosynthesized silver nanoparticles using berberis integerrima, Iran. J. Sci. Technol. Trans. A Sci. (2021) 1–11.
[47] K. Chand, C. Jiao, M.N. Lakhan, A.H. Shah, V. Kumar, D.E. Fouad, M.B. Chandio, A.A. Maitlo, M. Ahmed, D. Cao, Green synthesis, characterization and photocatalytic activity of silver nanoparticles synthesized with Nigella sativa seed extract, Chem. Phys. Lett. 763 (2021), 138218.
[48] F. Javadi, M.E.T. Yazdi, M. Baghani, A. Es-haghi, Biosynthesis, characterization of cerium oxide nanoparticles using Ceratonia siliqua and evaluation of antioxidant and cytotoxicity activities, Mater. Res. Express 6 (6) (2019), 065408.
[49] M. Modarres, M.E.T. Yazdi, Elicitation improves phenolic acid content and antioxidant enzymes activity in salvia leriifolia cell cultures, Iran. J. Sci. Technol. Trans. A Sci. (2021) 1–7.
[50] Y. Wang, A. Chinnathambi, O. Nasif, S.A. Alharbi, Green synthesis and chemical characterization of a novel anti-human pancreatic cancer supplement by silver nanoparticles containing Zingiber officinale leaf aqueous extract, Arab. J. Chem. 14 (4) (2021), 103081.
[51] M.A. Asghar, E. Zahir, S.M. Shahid, M.N. Khan, M.A. Asghar, J. Iqbal, G. Walker, Iron, copper and silver nanoparticles: green synthesis using green and black tea leaves extracts and evaluation of antibacterial, antifungal and aflatoxin B1 adsorption activity, LWT 90 (2018) 98–107.
[52] H.A. Yassa, S.M. George, A.E.R.M. Refaiy, E.M.A. Moneim, Camellia sinensis (green tea) extract attenuate acrylamide induced testicular damage in albino rats, Environ. Toxicol. 29 (10) (2014) 1155–1161.
[53] N.J. Naderi, M. Niakan, M.K. Fard, S. Zardi, Antibacterial activity of Iranian green and black tea on streptococcus mutans: an in vitro study, J. Dent. 8 (2) (2011) 55.
[54] Y.Y. Loo, B.W. Chieng, M. Nishibuchi, S. Radu, Synthesis of silver nanoparticles by using tea leaf extract from Camellia sinensis, Int. J. Nanomed. 7 (2012) 4263.
[55] D.A. Selvan, D. Mahendiran, R.S. Kumar, A.K. Rahiman, Garlic, green tea and turmeric extracts-mediated green synthesis of silver nanoparticles: phytochemical, antioxidant and in vitro cytotoxicity studies, J. Photochem. Photobiol. B Biol. 180 (2018) 243–252.
[56] N. Asare, C. Instanes, W.J. Sandberg, M. Refsnes, P. Schwarze, M. Kruszewski, G. Brunborg, Cytotoxic and genotoxic effects of silver nanoparticles in testicular cells, Toxicology 291 (1–3) (2012) 65–72.
[57] S.E. Fard, F. Tafvizi, M.B. Torbati, Silver nanoparticles biosynthesised using Centella asiatica leaf extract: apoptosis induction in MCF-7 breast cancer cell line, IET Nanobiotechnol. 12 (7) (2018) 994–1002.
[58] S.I. Abdel Wahab, A.B. Abdul, A.S. Alzubairi, M. Mohamed Elhassan, S. Mohan, In vitro ultramorphological assessment of apoptosis induced by zerumbone on (HeLa), J. Biomed. Biotechnol. 2009 (2009).
[59] R.A. Mahmoudian, M.M. Forghanifard, Crosstalk between MEIS1 and markers of different cell signaling pathways in esophageal squamous cell carcinoma, Mol. Biol. Rep. 47 (5) (2020) 3439–3448.
[60] R. Sharma, S. Gulati, S. Mehta, Preparation of gold nanoparticles using tea: a green chemistry experiment, J. Chem. Educ. 89 (10) (2012) 1316–1318.
[61] J. Singh, T. Dutta, K.-H. Kim, M. Rawat, P. Samddar, P. Kumar, 'Green'synthesis of metals and their oxide nanoparticles: applications for environmental remediation, J. Nanobiotechnol. 16 (1) (2018) 1–24.
[62] S.S.K. Kamal, P.K. Sahoo, J. Vimala, M. Premkumar, S. Ram, L. Durai, A novel green chemical route for synthesis of silver nanoparticles using Camellia sinensis, Acta Chim. Slov. 57 (2010) 808–812.
[63] V. Armendariz, I. Herrera, M. Jose-yacaman, H. Troiani, P. Santiago, J.L. Gardea-Torresdey, Size controlled gold nanoparticle formation by Avena sativa biomass: use of plants in nanobiotechnology, J. Nanopart. Res. 6 (4) (2004) 377–382.
[64] J.L. Gardea-Torresdey, E. Gomez, J.R. Peralta-Videa, J.G. Parsons, H. Troiani, M. Jose-Yacaman, Alfalfa sprouts: a natural source for the synthesis of silver nanoparticles, Langmuir 19 (4) (2003) 1357–1361.
[65] D. Sheny, J. Mathew, D. Philip, Phytosynthesis of Au, Ag and Au–Ag bimetallic nanoparticles using aqueous extract and dried leaf of Anacardium occidentale, Spectrochim. Acta Part A Mol. Biomol. Spectrosc. 79 (1) (2011) 254–262.
[66] L.A.P. Gontijo, E. Raphael, D.P.S. Ferrari, J.L. Ferrari, J.P. Lyon, M.A. Schiavon, pH effect on the synthesis of different size silver nanoparticles evaluated by DLS and their size-dependent antimicrobial activity, Matéria 25 (2020).
[67] A.O. Dada, F.A. Adekola, O.S. Adeyemi, O.M. Bello, A.C. Oluwaseun, O. J. Awakan, F.-A.A. Grace, Exploring the Effect of Operational Factors and Characterization Imperative to the Synthesis of Silver Nanoparticles, Silver Nanoparticles-Fabrication, Characterization and Applications, IntechOpen, 2018.
[68] H.M. Ibrahim, Green synthesis and characterization of silver nanoparticles using banana peel extract and their antimicrobial activity against representative microorganisms, J. Radiat. Res. Appl. Sci. 8 (3) (2015) 265–275.
[69] W. Zhang, X. Qiao, J. Chen, Synthesis of silver nanoparticles—effects of concerned parameters in water/oil microemulsion, Mater. Sci. Eng. B 142 (1) (2007) 1–15.
[70] M. Ghaemi, S. Gholamipoor, Controllable Synthesis and Characterization of Silver Nanoparticles Using Sargassum angostifolium, 2017.
[71] P. Phanjom, G. Ahmed, Effect of different physicochemical conditions on the synthesis of silver nanoparticles using fungal cell filtrate of Aspergillus oryzae (MTCC No. 1846) and their antibacterial effect, Adv. Nat. Sci. Nanosci. Nanotechnol. 8 (4) (2017), 045016.
[72] M. Khan, M.R. Shaik, S.F. Adil, S.T. Khan, A. Al-Warthan, M.R.H. Siddiqui, M. N. Tahir, W. Tremel, Plant extracts as green reductants for the synthesis of silver nanoparticles: lessons from chemical synthesis, Dalton Trans. 47 (35) (2018) 11988–12010.
[73] X.-H. Meng, N. Li, H.-T. Zhu, D. Wang, C.-R. Yang, Y.-J. Zhang, Plant resources, chemical constituents, and bioactivities of tea plants from the genus Camellia section Thea, J. Agric. Food Chem. 67 (19) (2018) 5318–5349.
[74] K. Ssekatawa, D. Byarugaba, C. Kato, E. Wampande, F. Ejobi, J. Nakavuma,M. Maaza, J. Sackey, E. Nxumalo, J. Kirabira, Physiochemical Properties Andantibacterial Activity of Silver Nanoparticles Green Synthesized by Camelliasinensis and Prunus africana Extracts, 2021.
[75] I.K. Siakavella, F. Lamari, D. Papoulis, M. Orkoula, P. Gkolfi, M. Lykouras, K. Avgoustakis, S. Hatziantoniou, Effect of plant extracts on the characteristics of silver nanoparticles for topical application, Pharmaceutics 12 (12) (2020) 1244.
[76] H.-M. Lin, S.-J. Tzeng, P.-J. Hsiau, W.-L. Tsai, Electrode effects on gas sensing properties of nanocrystalline zinc oxide, Nanostruct. Mater. 10 (3) (1998) 465–477.
[77] S.S. Shankar, A. Ahmad, R. Pasricha, M. Sastry, Bioreduction of chloroaurate ions by geranium leaves and its endophytic fungus yields gold nanoparticles of different shapes, J. Mater. Chem. 13 (7) (2003) 1822–1826.
[78] M.N. Nadagouda, N. Iyanna, J. Lalley, C. Han, D.D. Dionysiou, R.S. Varma, Synthesis of silver and gold nanoparticles using antioxidants from blackberry, blueberry, pomegranate, and turmeric extracts, ACS Sustain. Chem. Eng. 2 (7) (2014) 1717–1723.
[79] M.E.T. Yazdi, M.S. Amiri, H.A. Hosseini, R.K. Oskuee, H. Mosawee, K. Pakravanan, M. Darroudi, Plant-based synthesis of silver nanoparticles in Handelia trichophylla and their biological activities, Bull. Mater. Sci. 42 (4) (2019) 155.
[80] İ. Gülçin, The antioxidant and radical scavenging activities of black pepper (Piper nigrum) seeds, Int. J. Food Sci. Nutr. 56 (7) (2005) 491–499.
[81] Z. Bedlovičová, I. Strapáč, M. Baláž, A. Salayová, A brief overview on antioxidant activity determination of silver nanoparticles, Molecules 25 (14) (2020) 3191.
[82] S. Patil, P. Rajiv, R. Sivaraj, An investigation of antioxidant and cytotoxic properties of green synthesized silver nanoparticles, INDO Am. J. Pharm. Sci. 2 (10) (2015) 1453–1459.
[83] S. Bhakya, S. Muthukrishnan, M. Sukumaran, M. Muthukumar, Biogenic synthesis of silver nanoparticles and their antioxidant and antibacterial activity, Appl. Nanosci. 6 (5) (2016) 755–766.
[84] M.S. Blois, Antioxidant determinations by the use of a stable free radical, Nature 181 (4617) (1958) 1199–1200.
[85] C. Shanmugam, G. Sivasubramanian, B. Parthasarathi, K. Baskaran, R. Balachander, V. Parameswaran, Antimicrobial, free radical scavenging activities and catalytic oxidation of benzyl alcohol by nano-silver synthesized from the leaf extract of Aristolochia indica L.: a promenade towards sustainability, Appl. Nanosci. 6 (5) (2016) 711–723.

[86] A. Magdy, E. Sadaka, N. Hanafy, M.A. El-Magd, N. Allahloubi, M. El Kemary, Green tea ameliorates the side effects of the silver nanoparticles treatment of Ehrlich ascites tumor in mice, Mol. Cell. Toxicol. 16 (3) (2020) 271–282.
[87] R. Vivek, R. Thangam, K. Muthuchelian, P. Gunasekaran, K. Kaveri, S. Kannan, Green biosynthesis of silver nanoparticles from Annona squamosa leaf extract and its in vitro cytotoxic effect on MCF-7 cells, Process Biochem. 47 (12) (2012) 2405–2410.
[88] K. Venugopal, H. Rather, K. Rajagopal, M. Shanthi, K. Sheriff, M. Illiyas, R. Rather, E. Manikandan, S. Uvarajan, M. Bhaskar, Synthesis of silver nanoparticles (Ag NPs) for anticancer activities (MCF 7 breast and A549 lung cell lines) of the crude extract of Syzygium aromaticum, J. Photochem. Photobiol. B Biol. 167 (2017) 282–289.
[89] P. Asharani, M.P. Hande, S. Valiyaveettil, Anti-proliferative activity of silver nanoparticles, BMC Cell Biol. 10 (1) (2009) 1–14.
[90] P. AshaRani, G. Low Kah Mun, M.P. Hande, S. Valiyaveettil, Cytotoxicity and genotoxicity of silver nanoparticles in human cells, ACS Nano 3 (2) (2009) 279–290.
[91] T. Zhang, L. Wang, Q. Chen, C. Chen, Cytotoxic potential of silver nanoparticles, Yonsei Med. J. 55 (2) (2014) 283–291.
[92] K.V. Naveen, K. Saravanakumar, A. Sathiyaseelan, M.-H. Wang, Eco-friendly synthesis and characterization of Aloe vera/Gum Arabic/silver nanocomposites and their antibacterial, antibiofilm, and wound healing properties, Colloid Interface Sci. Commun. 46 (2022), 100566.
[93] K.V. Naveen, H.-Y. Kim, K. Saravanakumar, A.V.A. Mariadoss, M.-H. Wang, Phyto-fabrication of biocompatible silver nanoparticles using Potentilla chinensis Ser leaves: characterization and evaluation of its antibacterial activity, J. Nanostruct. Chem. (2021) 1–13.
[94] C. Krishnaraj, P. Muthukumaran, R. Ramachandran, M. Balakumaran, P. Kalaichelvan, Acalypha indica Linn: biogenic synthesis of silver and gold nanoparticles and their cytotoxic effects against MDA-MB-231, human breast cancer cells, Biotechnol. Rep. 4 (2014) 42–49.
[95] L. Inbathamizh, T.M. Ponnu, E.J. Mary, In vitro evaluation of antioxidant and anticancer potential of Morinda pubescens synthesized silver nanoparticles, J. Pharm. Res. 6 (1) (2013) 32–38.
[96] R.U. Janicke, M.L. Sprengart, M.R. Wati, A.G. Porter, Caspase-3 is required for DNA fragmentation and morphological changes associated with apoptosis, J. Biol. Chem. 273 (16) (1998) 9357–9360.
[97] R. Hu, K.-T. Yong, I. Roy, H. Ding, S. He, P.N. Prasad, Metallic nanostructures as localized plasmon resonance enhanced scattering probes for multiplex dark-field targeted imaging of cancer cells, J. Phys. Chem. C 113 (7) (2009) 2676–2684.
[98] M. MacFarlane, A.C. Williams, Apoptosis and Disease: A Life Or Death Decision: Conference and Workshop on Apoptosis and Disease, John Wiley & Sons, Ltd, Chichester, UK, 2004.
[99] M.B. Vahideh Mohammadzadeh, Mohammad Sadegh Amiri, Mohammad Ehsan Taghavizadeh Yazdi, Mohadeseh Hassanisaadi, Abbas Rahdar, Rajender S. Varma. Applications of Plant-based Nanoparticles in Nanomedicine: A Sustainable Chemistry and Pharmacy, 2022.
[100] J.M. Adams, S. Cory, Life-or-death decisions by the Bcl-2 protein family, Trends Biochem. Sci. 26 (1) (2001) 61–66.
[101] J.-C. Martinou, D.R. Green, Breaking the mitochondrial barrier, Nat. Rev. Mol. Cell Biol. 2 (1) (2001) 63–67.
[102] C. Jalili, M.R. Salahshoor, M.T. Moradi, M. Ahookhash, M. Taghadosi, M. Sohrabi, Expression changes of apoptotic genes in tissues from mice exposed to nicotine, Asian Pac. J. Cancer Prev. APJCP 18 (1) (2017) 239.
[103] B. Morak-Młodawska, K. Pluta, M. Latocha, M. Jeleń, D. Kuśmierz, Synthesis, anticancer activity, and apoptosis induction of novel 3, 6-diazaphenothiazines, Molecules 24 (2) (2019) 267.
[104] B. Mousavi, F. Tafvizi, S. Zaker, Bostanabad, Green synthesis of silver nanoparticles using Artemisia turcomanica leaf extract and the study of anti-cancer effect and apoptosis induction on gastric cancer cell line (AGS), Artif. Cells Nanomed. Biotechnol. (2018) 1–12.
[105] R. Maity, M. Chatterjee, A. Banerjee, A. Das, R. Mishra, S. Mazumder, N. Chanda, Gold nanoparticle-assisted enhancement in the anti-cancer properties of theaflavin against human ovarian cancer cells, Mater. Sci. Eng. C 104 (2019), 109909.
[106] S.-B. Lee, S. Lee, J.-Y. Park, S.-Y. Lee, H.-S. Kim, Induction of p53-dependent apoptosis by prostaglandin A2, Biomolecules 10 (3) (2020) 492.
[107] H. Carr, Repositioning Aspirin and Metformin to Improve Prostate Cancer Treatment and Outcome, University of Bristol, 2019.
[108] K. Hientz, A. Mohr, D. Bhakta-Guha, T. Efferth, The role of p53 in cancer drug resistance and targeted chemotherapy, Oncotarget 8 (5) (2017) 8921.
[109] T. Mitupatum, K. Aree, S. Kittisenachai, S. Roytrakul, S. Puthong, S. Kangsadalampai, P. Rojpibulstit, mRNA expression of Bax, Bcl-2, p53, cathepsin B, caspase-3 and caspase-9 in the HepG2 cell line following induction by a novel monoclonal Ab Hep88 mAb: cross-talk for paraptosis and apoptosis, Asian Pac. J. Cancer Prev. 17 (2) (2016) 703–712.
[110] F. Mobaraki, M. Seghatoleslam, A. Fazel, A. Ebrahimzadeh-Bideskan, Effects of MDMA (ecstasy) on apoptosis and heat shock protein (HSP70) expression in adult rat testis, Toxicol. Mech. Methods 28 (3) (2018) 219–229.
[111] M.E.T. Yazdi, M.S. Amiri, F. Nourbakhsh, M. Rahnama, F. Forouzanfar, S. H. Mousavi, Bio-indicators in cadmium toxicity: role of HSP27 and HSP70, Environ. Sci. Pollut. Res. (2021) 1–21.
[112] H. Zhang, W. Chen, C.-J. Duan, C.-F. Zhang, Overexpression of HSPA2 is correlated with poor prognosis in esophageal squamous cell carcinoma, World J. Surg. Oncol. 11 (1) (2013) 1–8.